Probing Site Specificity of DNA Binding Metallointercalators by NMR Spectroscopy and Molecular Modeling†

Emma M. Proudfoot,‡ Joel P. Mackay,§ and Peter Karuso*,‡

Department of Chemistry, Macquarie University, Sydney, NSW 2109, Australia, and Department of Biochemistry, University of Sydney, Sydney, NSW 2006, Australia

Received July 17, 2000; Revised Manuscript Received December 12, 2000

ABSTRACT: The molecular recognition of oligonucleotides by chiral ruthenium complexes has been probed by NMR spectroscopy using the template Δ-*cis*-α- and Δ-*cis*-*β*-[Ru(*RR*-picchxnMe$_2$) (bidentate)]$^{2+}$, where the bidentate ligand is one of *phen* (1,10-phenanthroline), *dpq* (dipyrido[3,2-*f*:2′,3′-*h*]quinoxaline), or *phi* (9,10-phenanthrenequinone diimine) and *picchxnMe$_2$* is *N*,*N*′-dimethyl-*N*,*N*′-di(2-picolyl)-1,2-diaminocyclohexane. By varying only the bidentate ligand in a series of complexes, it was shown that the bidentate alone can alter binding modes. DNA binding studies of the Δ-*cis*-α-[Ru(*RR*-picchxnMe$_2$)(phen)]$^{2+}$ complex indicate fast exchange kinetics on the chemical shift time scale and a "partial intercalation" mode of binding. This complex binds to [d(CGCGATCGCG)]$_2$ and [d(ATATCGATAT)]$_2$ at AT, TA, and GA sites from the minor groove, as well as to the ends of the oligonucleotide at low temperature. Studies of the Δ-*cis*-*β*-[Ru(*RR*-picchxnMe$_2$)(phen)]$^{2+}$ complex with [d(CGCGATCGCG)]$_2$ showed that the complex binds only weakly to the ends of the oligonucleotide. The interaction of Δ-*cis*-α-[Ru(*RR*-picchxnMe$_2$)-(dpq)]$^{2+}$ with [d(CGCGATCGCG)]$_2$ showed intermediate exchange kinetics and evidence of minor groove intercalation at the GA base step. In contrast to the *phen* and *dpq* complexes, Δ-*cis*-α- and Δ-*cis*-*β*-[Ru-(*RR*-picchxnMe$_2$)(phi)]$^{2+}$ showed evidence of major groove binding independent of the metal ion configuration. DNA stabilization induced by complex binding to [d(CGCGATCGCG)]$_2$ (measured as ΔT_m) increases in the order *phen* < *dpq* and DNA affinity in the order *phen* < *dpq* < *phi*. The groove binding preferences exhibited by the different bidentate ligands is explained with the aid of molecular modeling experiments.

Because DNA acts as the template from which all protein synthesis takes place, the development of high-affinity, sequence-specific DNA binding agents represents one of the major challenges of rational drug design. An understanding of how the handful of DNA specific drugs target specific sites will lead to novel therapeutic agents and the development of sensitive molecular probes. Consequently, much effort has been focused on the synthesis and characterization of small molecules which display a capacity to bind DNA in this manner. Chiral, octahedral ruthenium complexes containing planer aromatic ligands have been used in a wide range of such studies, although in some cases, the interpretation of these results has been controversial (*1*).

Tris-bidentate complexes containing the *phen*[1] (1,10-phenanthroline) ligand (Figure 1) are among the most widely studied to date, but there have been conflicting interpretations of the mode of DNA binding exhibited by such complexes. An early study concluded, on the basis of ^{1}H NMR data, that Δ-[Ru(phen)$_3$]$^{2+}$ binds intercalatively from the major groove, while the Λ-isomer binds to the surface of the minor groove (*2*). In contrast, like studies have indicated minor groove nonintercalative binding for both Δ- and Λ-[Ru-(phen)$_3$]$^{2+}$ in the AT region of [d(CGCGATCGCG)]$_2$ (*3*−*5*). Furthermore, a recent ^{1}H NMR study indicated minor groove partially intercalative binding for the same complex in the C_8C_9 region of [d(TCGGGATCCCGA)]$_2$ (*6*). Other techniques, including linear, circular, and electronic dichroism, molecular modeling, absorption, fluorescence, and luminescence spectroscopies, used to study Δ- and Λ-[Ru-(phen)$_3$]$^{2+}$, propose a variety of interactions with DNA, including both intercalation and nonintercalation, with either AT or GC selectivity, depending on the chirality of the complex (*7*−*11*).

Larger bidentate ligands have been substituted for *phen* in these complexes in attempts to increase their binding

† This research was supported by the Australian Research Council, large grant A29600959.

* Corresponding author. Phone: (612) 9850 8290. Fax: (612) 9850 8313. E-mail: Peter.Karuso@mq.edu.au.

‡ Macquarie University.

§ University of Sydney.

[1] Abbreviations: *picchxnMe$_2$*, *N*,*N*′-dimethyl-*N*,*N*′-di(2-picolyl)-1,2-diaminocyclohexane; *phen*, 1,10-phenanthroline; *dpq*, dipyrido[3,2-*f*:2′,3′-*h*]quinoxaline; *phi*, 9,10-phenanthrenequinone diimine; *dppz*, dipyrido[3,2-*a*:2′,3′-*c*]phenazine; *bpy*, 2,2′-bipyridine; *en*, 1,2-ethylenediamine; α-*phen*, Δ-*cis*-α-[Ru(*RR*-picchxnMe$_2$)(phen)]$^{2+}$; *β*-*phen*, Δ-*cis*-*β*-[Ru(*RR*-picchxnMe$_2$)(phen)]$^{2+}$; α-*dpq*, Δ-*cis*-α-[Ru(*RR*-picchxnMe$_2$)(dpq)]$^{2+}$; *β*-*dpq*, Δ-*cis*-*β*-[Ru(*RR*-picchxnMe$_2$)(dpq)]$^{2+}$; α-*phi*, Δ-*cis*-α-[Ru(*RR*-picchxnMe$_2$)(phi)]$^{2+}$; *β*-*phi*, Δ-*cis*-*β*-[Ru(*RR*-picchxnMe$_2$)(phi)]$^{2+}$; DQF-COSY, double-quantum-filtered correlation spectroscopy; ROESY, rotating frame nuclear Overhauser and exchange spectroscopy; NOESY, nuclear Overhauser and enhancement spectroscopy; TOCSY, total correlation spectroscopy; ESFF, extensible systematic force field; τ_m, mixing time; MM, molecular mechanics; MD, molecular dynamics.

10.1021/bi001655f CCC: $20.00
Published on Web 03/16/2001

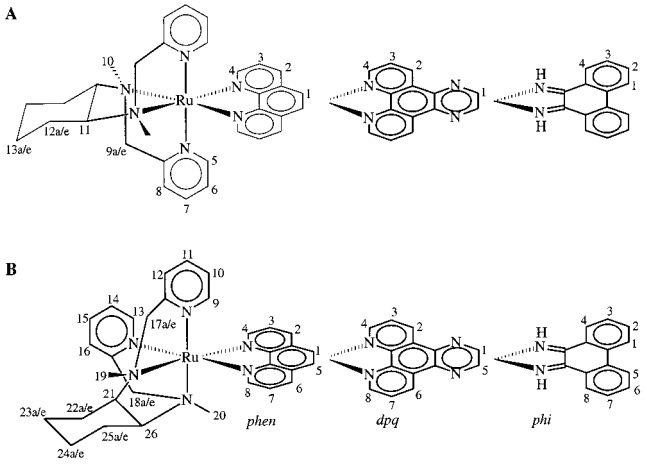

FIGURE 1: Structure of (A) Δ-*cis*-α-[Ru(*RR*-picchxnMe$_2$)(L)]$^{2+}$ and (B) Δ-*cis*-*β*-[Ru(*RR*-picchxnMe$_2$)(L)]$^{2+}$, where L = *phen*, *dpq*, or *phi*, showing the ^{1}H labeling schemes.

affinity for DNA (through increased aromatic overlap with DNA bases) and potentially to modulate their DNA sequence specificity. Two recent ^{1}H NMR studies exploring the *dpq* ligand (*12*, *13*) (dipyrido[3,2-*f*:2′,3′-*h*]quinoxaline, Figure 1), which incorporates an additional pyrazine ring, show Δ-[Ru(phen)$_2$dpq]$^{2+}$ to intercalate into DNA from the minor groove, via insertion of the *dpq* ligand at purine−purine/pyrimidine−pyrimidine sites (*6*, *13*). Intercalation from both the major (*14*−*16*) and the minor (*4*, *17*) grooves has been proposed for the extended ligand *dppz* (dipyrido[3,2-*a*:2′,3′-*c*]phenazine), which contains an additional quinoxaline ring compared to *phen*. These varying results further highlight the uncertainty that exists regarding the binding of these types of compounds to DNA.

In contrast, complexes containing the *phi* ligand (9,10-phenanthrenequinone diimine, Figure 1) have been reported to intercalate only from the major groove. The established dogma is that Δ-enantiomers show preferences for GC/CG sequence selectivity, and several ^{1}H NMR studies on complexes of this ligand have been carried out to date to verify this, including a preliminary NMR solution structure of a rhodium complex bound to an oligonucleotide (*18*) and the corresponding X-ray structure (*19*). More varied results have been obtained for the Λ-enantiomers, including major groove intercalation at a TG site (*20*), a TA site (*21*), and a TX site (*22*), as well as sequence neutral intercalation (*23*), depending on the ancillary ligands.

The lack of general consensus in octahedral metal complex−DNA binding studies reflects both the application of indirect techniques that may be interpreted in various ways and the variable role played by ancillary ligands in groove recognition and selectivity. In an effort to establish predictability for those factors that govern groove and sequence selectivity, we have undertaken a study of a series of complexes based on the Δ-[Ru(picchxnMe$_2$)(bidentate)]$^{2+}$ template (*24*, *25*) [*picchxnMe*$_2$ is *N*,*N*′-dimethyl-*N*,*N*′-di(2-picolyl)-1,2-diaminocyclohexane (*26*); Figure 1]. In this study, the stereochemistry of the *Ru-picchxnMe*$_2$ moiety and the nature of the bidentate ligand (*phen*, *dpq*, *phi*) have been varied. Using direct evidence from one- and two-dimensional NMR spectroscopy, we have identified both the sequence and groove selectivity of these complexes, while molecular modeling of the complexes bound to DNA has allowed us to postulate a general theory to explain groove specificity based on characteristics of the bidentate ligand alone.

MATERIALS AND METHODS

Metal Complex and Oligonucleotide Synthesis. The synthesis and characterization of the Δ-*cis*-α- and Δ-*cis*-*β* complexes (*27*) will be described elsewhere. The α- and *β*-isomers of all three complexes were separated by column chromatography on SP-Sephadex C-25 cation-exchange resin using an increasing gradient of NaCl.

[d(CGCGATCGCG)]$_2$ and [d(ATATCGATAT)]$_2$ were synthesized on an Applied Biosystems DNA synthesizer (Model 391) using phosphoramidite chemistry (10 μmol scale, trityl-on) and purified by reverse-phase HPLC. The oligonucleotides were detritylated and converted into the Na$^+$ form by treatment with 80% acetic acid and 3 M sodium acetate, respectively.

Sample Preparation for NMR Spectroscopy. Each oligonucleotide sample was buffered in 10 mM sodium phosphate, pD 7.0 (uncorrected for isotope effects), containing 10 mM NaCl and 0.01% NaN_3. d_4-Trimethylsilylpropionic acid (TSP) was added as an internal chemical shift reference, and all NMR shifts were recorded relative to TSP (0.00 ppm). The DNA was annealed in the NMR tube by heating to 90 °C in a water bath, followed by cooling to room temperature over several hours. Sample concentrations were quantified by measuring the absorbance (optical density unit, ODU) of a 1 mL solution at 260 nm (20 °C), using the UV spectrophotometric method of Sambrook (*28*), where 1 ODU corresponds to 33 μg/mL of single-stranded DNA and 50 μg/mL of double-stranded DNA. The concentration of each sample was 1−3 mM duplex DNA and is specified in the relevant figure captions. All DNA and complex samples were exchanged twice with D_2O (99.9%, Aldrich) and then made up to 500 μL with D_2O (99.96%, Aldrich).

Acquisition of NMR Data. NMR spectra were acquired on Varian XL400 (400 MHz), Bruker AMX600 (600 MHz), and Bruker DMX600 (600 MHz) spectrometers. One-dimensional (1D) ^{1}H spectra were recorded with either 16K or 32K data points with relaxation delays of 1−2 s. Spectral widths were adjusted to allow at least 1 ppm either side of the observable resonances, and the carrier frequency was set to the frequency of the water signal. Suppression of the solvent signal was generally achieved by selective irradiation during the relaxation delay. All two-dimensional (2D) spectra were recorded with quadrature detection in both dimensions using time proportional phase incrementation (TPPI). For DQF-COSY and ROESY experiments, 2K data points were collected in t_2 and 512 in t_1 with 24−80 scans per t_2 increment.

Data were processed using the Bruker XWinNMR (version 1.3) software. The spectra were zero-filled twice in F_1 and once in F_2 and processed with either squared sine-bell (π/2- or π/3-shifted) or Lorentzian−Gaussian window functions. The spectra were referenced and phased in both dimensions, and baseline correction was subsequently applied in F_2. If necessary, t_1 noise was subtracted using the Bruker program Aurelia (version 2.0.6).

NMR resonances of the unbound α- and *β*-ruthenium complexes were assigned using a combination of DQF-COSY and compensated ROESY spectra. Assignment of free

DNA resonances was carried out using DQF-COSY, TOCSY, and NOESY spectra. The Δ-*cis*-α-[Ru(*RR*-picchxnMe$_2$)(dpq)]$^{2+}$ complex was found to be photosensitive, so sample solutions were stored in complete darkness. In contrast, the closely related *phen* complexes were completely stable to ambient light.

1D NMR titrations were carried out for each complex−DNA adduct. The Ru complexes were added in aliquots to oligonucleotide samples in the NMR tube to a maximum complex:duplex ratio (R) of 3.5. The complex was added in increments of 0.1 molar equiv, and a ^{1}H NMR spectrum was recorded after each addition. For complex additions above $R = 1.0$, the complex was added in increments of 0.2−0.5 molar equiv. Temperatures were held constant throughout the course of the titrations and are specified in the relevant figure captions for each experiment. For the final high-R solution, 2D NOESY ($\tau_m = 100-400$ ms), DQF-COSY, and TOCSY ($\tau_m = 30-90$ ms) spectra were collected. NMR spectroscopy was used to measure the melting point (or helix-to-coil transition; T_m) temperature of [d(CGCGATCGCG)]$_2$ in the presence and absence of metal complexes by following the T_6CH_3 resonance (0−95 °C) and fitting the observed chemical shift to either a four-parameter or six-parameter sigmoidal curve (*29*).

Binding Constant Determination. Association constants were calculated by monitoring the chemical shift of a selected DNA resonance (δ_{obs}) with increasing complex concentration and using the relationship (*30*):

$$\delta_{obs} = \left(\frac{A_{TOT} - x}{A_{TOT}}\right)\delta_A + \left(\frac{x}{A_{TOT}}\right)\delta_{AB} \qquad (1)$$

where A_{TOT} is the total concentration of duplex DNA, x is the concentration of DNA bound to the ruthenium complex, and δ_A and δ_{AB} are the limiting chemical shifts of the selected proton of interest in the free and bound forms, respectively. Data were fitted to this equation using the nonlinear least squares algorithm in KaleidaGraph (version 3.0.1, Abelbeck Software, 1993). The binding constant (K_b) was calculated from x by the relationship:

$$K_b = \frac{x}{(A_{TOT} - x)(B_{TOT} - x)} \qquad (2)$$

where B_{TOT} is the total concentration of the Ru complex.

Molecular Modeling. A 3D energy-minimized model of a portion of the Δ-*cis*-α-[Ru(*RR*-picchxnMe$_2$)(dpq)]$^{2+}$−[d(CGCGATCGCG)]$_2$ adduct was constructed using the Insight II/Discover3 molecular modeling system (version 97.0, Molecular Simulations Inc., 1997). The oligonucleotide fragment 5′-CGAT-3′ was modified from the intercalation site of an actinomycin D−oligonucleotide crystal structure (*31*). The complex was built using the builder module in InsightII, energy minimized briefly (quasi-Newton−Raphson algorithm), and inserted into the intercalation site from the minor groove at the 5′-GA-3′ base step manually. Solvent was simulated with a distance-dependent dielectric ($\epsilon = 4r_{ij}$), and a cutoff of 20 Å was used for nonbonded interactions with a switching distance of 1.5 Å. Nine DNA−complex distance restraints consistent with the observed intermolecular NOEs (40 °C, $R = 3.5$) were included in the minimization. The NOEs were not integrated as all were of approximately equal volume and no convenient reference cross-peak could be found. Each was assigned a distance between 1.8 and 5.0 Å, consistent with the distances measurable by NMR spectroscopy. These restraints were applied using a flat-bottomed potential, with an energy penalty of 100 kcal mol^{-1} Å^{-2} applied outside the upper (5.0 Å) and lower (1.8 Å) restraint boundaries and no energy penalty (beyond the force field) within the restraint boundaries. The ESFF force field, which is parametrized for octahedral coordinate Ru(II) (*32*, *33*) was used in all Discover3 calculations. The starting structure was subjected to 1000 iterations of steepest descent minimization, followed by conjugate gradient energy minimization until a maximum derivative of less than 0.01 kcal mol^{-1} Å^{-2} was achieved. The minimized structure was subjected to a MD−MM protocol consisting of 2 ns of dynamics (273 K) with no NOE restraints but fixed DNA, saving a structure every 10 ps. Each of the 200 high energy structures was minimized (as above) with NOE restraints on and DNA atom positions fixed. A final round of minimization with no NOE restraints and free DNA (except the interstrand H-bonds, which were tethered; 1−2 Å, 100 kcal mol^{-1} Å^{-2}) produced 200 low-energy structures. The nine lowest energy structures were superimposed and found to be identical.

RESULTS

Five different ruthenium complexes have been used in this study: Δ-*cis*-α-[Ru(*RR*-picchxnMe$_2$)(phen)]$^{2+}$ (α-*phen*), Δ-*cis*-*β*-[Ru(*RR*-picchxnMe$_2$)(phen)]$^{2+}$ (*β*-*phen*), Δ-*cis*-α-[Ru(*RR*-picchxnMe$_2$)(dpq)]$^{2+}$ (α-*dpq*), Δ-*cis*-α-[Ru(*RR*-picchxnMe$_2$)(phi)]$^{2+}$ (α-*phi*), and Δ-*cis*-*β*-[Ru(*RR*-picchxnMe$_2$)(phi)]$^{2+}$ (*β*-*phi*). Using 1D and 2D ^{1}H NMR spectroscopy, their binding to two different DNA sequences was examined, namely, [d(CGCGATCGCG)]$_2$ and [d(ATATCGATAT)]$_2$. Each oligonucleotide offers either a single embedded GpC or ApT intercalation site.

A combination of DQF-COSY, compensated ROESY, and chemical shift information was used to assign the ^{1}H NMR spectra of the free ruthenium complexes. In the aliphatic region of the α-complexes, H11 was the most deshielded proton. DQF-COSY correlations allowed the complete assignment of the remaining spin system. Equatorial and axial protons were distinguished on the basis of the size of the coupling constants and confirmed from the respective ROESY spectrum. In the picolyl spin system, H5 (ortho to ring N) was the furthest downfield and showed ROEs to the methyl groups (H10). H8 showed ROEs to both protons on C9, and DQF-COSY correlations identified the remaining protons in the spin system. Similarly, H4 of the bidentate was assigned on the basis of chemical shift and the remaining signals on the basis of scalar couplings. The Δ absolute configuration was confirmed through quantitative ROE measurements (*24*). For the *β*-complexes, assignment was begun with H20, the most shielded methyl group, which is positioned under the large bidentate ligand. This methyl gave ROEs to H26, H18a, and H18e. The remaining cyclohexyl protons were assigned on the basis of COSY correlations. H18e, in turn, displayed an ROE to H16, and in a similar fashion, H17a was correlated to H12 and H19, allowing assignment of the picolyl protons. DNA assignments were achieved through literature methods and the structures

Table 1: ^{1}H NMR Chemical Shift Changes in Ru Complex Aromatic Protons When Bound to [d(CGCGATCGCG)]$_2$[a]

α-complex protons	$\delta_B - \delta_F$ α-*phen* (ppm)	$\delta_B - \delta_F$ α-*dpq* (ppm)	$\delta_B - \delta_F$ α-*phi* (ppm)	β-complex protons	$\delta_B - \delta_F$ β-*phen* (ppm) (0 °C, 2:1)
bidentate				bidentate	
H1	−1.23	−0.83	−0.82	H1, H5	−0.41, −0.44
H2	−1.04	−1.01	−0.67	H2, H6	−0.17, −0.36
H3	−0.62	−0.68	−0.45	H3, H7	−0.24, −0.20
H4	−0.29	−0.21	−0.44	H4, H8	−0.35, −0.16
imine[b]			−0.14		
picolyl				picolyl	
H5	−0.13	0.01	−0.01	H9, H13	−0.07, −0.11
H6	0.03	0.10	0.06	H10, H14	0.02, −0.03
H7	−0.01	0.06	0.02	H11, H15	−0.02, −0.03
H8	−0.07	0.00	0.01	H12, H16	−0.06, −0.06

[a] Data were recorded at ~2 mM complex and DNA at 40 °C in buffered D_2O at a complex:duplex ratio of 1:1 unless otherwise stated. δ_B = chemical shift of bound complex, and δ_F = chemical shift of free complex under the same buffer, temperature, and solvent conditions. Negative numbers indicate an upfield shift. [b] Data recorded at 20 °C in 90% H_2O/10% D_2O.

confirmed as regular B-DNA on the basis of strong correlations between each base H6/8 proton and its own H″ proton (*34*).

Δ-*cis*-α-*[Ru(RR-picchxnMe$_2$)(phen)]$^{2+}$−[d(CGCGATCGCG)]$_2$ Adduct.* In a preliminary report, we have previously shown that a ^{1}H NMR titration of α-*phen* against [d(CGCGATCGCG)]$_2$ at 40 °C reveals substantial changes in the chemical shifts of specific DNA resonances (*24*). Most significantly, there is a marked upfield shift of minor groove resonances, in particular, A_5H2. At a 1:1 complex:duplex ratio, this proton resonance is shifted 0.29 ppm upfield in comparison to free DNA. A simultaneous but less significant (up to 0.09 ppm) downfield shift of the major groove A_5H8, C_7H6, and T_6H6 proton signals occurs. The proton resonances on the *phen* ligand also undergo concomitant upfield shifts compared to the free complex in solution (Table 1), consistent with substantial shielding by the duplex. The *phen* protons are affected in the order H1 > H2 > H3 > H4. In contrast, the *picchxnMe$_2$* proton chemical shifts are only slightly affected, as demonstrated by the picolyl chemical shift changes listed in Table 1.

To ascertain where on the oligonucleotide the complex binds and from which groove, the chemical shift differences ($\delta_B - \delta_F$) have been plotted for minor groove (H1′ and AH2) and major groove (H6, H8, CH5, and TCH_3) protons. Where an individual base has more than one proton in the major or minor groove, an average value of the change in chemical shift was used. Figure 2 shows the data recorded at both 30 °C (A) and 0 °C (B), highlighting the differences in binding characteristics at the two temperatures. At 30 °C, the largest effect is the observed shielding of the oligonucleotide protons in the 5′-GAT-3′ region of the minor groove and, to a lesser extent, the complementary deshielding of the 3′-CTA-5′ region in the major groove. However, at 0 °C there are also significant chemical shift changes at the terminal base pairs, C_9•G_2 and G_{10}•C_1, and a decrease in the effect on the central region of the oligonucleotide. This implies that the Ru complex has been redistributed along the oligonucleotide at 0 °C, between the central and terminal binding sites.

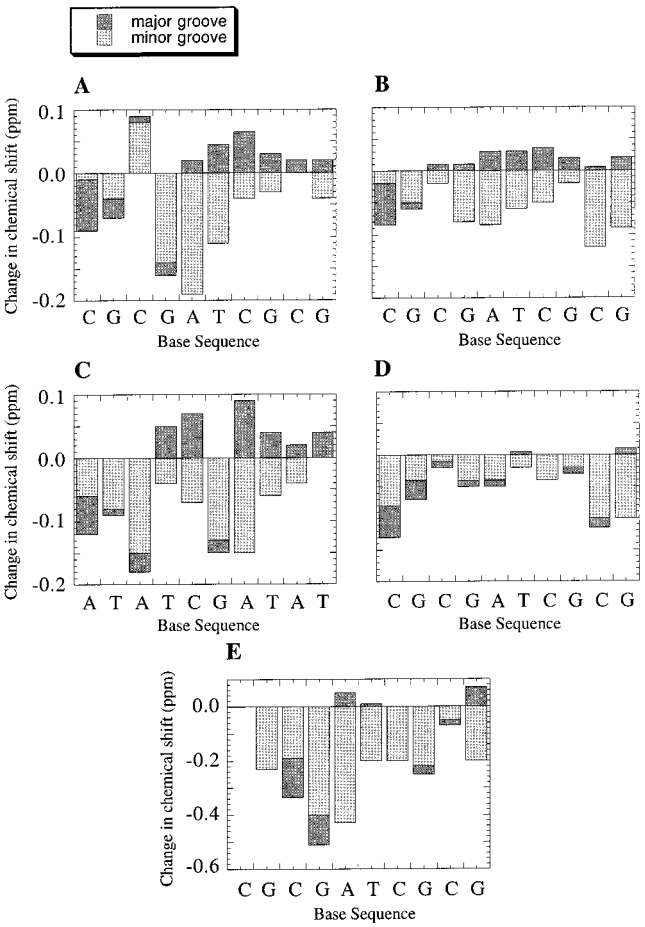

FIGURE 2: Changes in chemical shift ($\delta_B - \delta_F$) for oligonucleotide major (H6, H8, CH5, and TCH_3) and minor (H1′ and AH2) groove protons in the presence of the Ru complex. δ_B = chemical shift of bound DNA, and δ_F = chemical shift of free DNA under the same buffer, temperature, and solvent conditions. Negative numbers indicate an upfield shift. Panels: (A) α-*phen*−[d(CGCGATCGCG)]$_2$, 30 °C, 1:1 complex:duplex ratio; (B) α-*phen*−[d(CGCGATCGCG)]$_2$, 0 °C, 1:1; (C) α-*phen*−[d(ATATCGATAT)]$_2$, 40 °C, 1:1; (D) β-*phen*−[d(CGCGATCGCG)]$_2$, 0 °C, 2:1; (E) α-*dpq*−[d(CGCGATCGCG)]$_2$, 40 °C, 3.5:1.

The patterns of intermolecular NOEs observed in NOESY spectra recorded at both 30 and 0 °C (Figure 3) confirmed that the central GATC sequence is the predominant region to which binding occurs (*24*). At 30 °C, 25 intermolecular NOEs were observed, mostly between the aromatic complex protons and the minor groove DNA protons H1′ and A_5H2. A complete list of intermolecular NOEs to the central and terminal DNA regions is available in Supporting Information. The NOESY spectra also revealed that the G_4H1′-A_5H8, A_5-H1′-T_6H6, and T_6H1′-C_7H6 cross-peaks are not significantly reduced in intensity upon binding to the complex.

Δ-*cis*-α-*[Ru(RR-picchxnMe$_2$)(phen)]$^{2+}$−[d(ATATCGATAT)]$_2$ Adduct.* To further clarify the binding preferences of the α-*phen* complex, a similar study was undertaken with the DNA sequence [d(ATATCGATAT)]$_2$. This sequence has a single CG central site and a variety of possible AT binding sites. A ^{1}H NMR titration of this oligonucleotide with α-*phen* at 25 °C (see Supporting Information) revealed an immediate broadening of the A_7H2, A_7H8, and T_4CH_3 resonances, and at a 1:1 ratio, significant broadening extended throughout the spectrum. 2D TOCSY and NOESY spectra recorded at 40 °C resulted in faster exchange and sharper lines, allowing

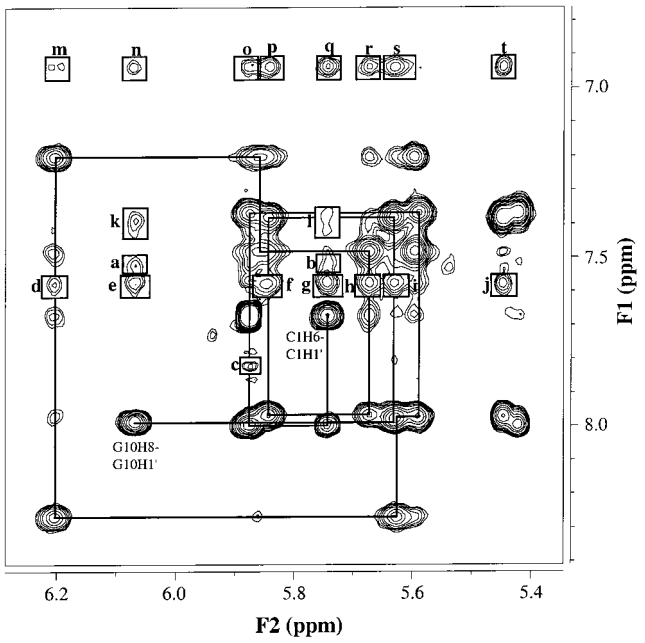

FIGURE 3: Portion of a ^{1}H NOESY spectrum (τ_m = 400 ms) of the α-*phen*−[d(CGCGATCGCG)]$_2$ adduct at a 1:1 ratio (1.25 mM) at 0 °C. The solid line indicates the H1′-H6/H8 sequential correlations observed along the duplex, while the intermolecular NOEs between the complex and the duplex are shown in boxes. The labels correspond to NOEs between the following protons: (a) H3-G_{10}-H1′, (b) H3-C_1H1′, (c) H2-C_1H5 (d) H7-A_5H1′, (e) H7-G_{10}H1′, (f) H7-T_6H1′/G_8H1′, (g) H7-C_1H1′, (h) H7-C_7H1′, (i) H7-G_4H1′/C_9-H1′, (j) H7-C_9H5, (k) H8-G_{10}H1′, (l) H8-C_1H1′, (m) H6-A_5H1′, (n) H6-G_{10}H1′, (o) H6-C_1H5, (p) H6-T_6H1′/G_8H1′, (q) H6-C_1H1′, (r) H6-C_7H1′, (s) H6-G_4H1′/C_9H1′, and (t) H6-C_9H5. The assignments for (f), (i), (p), and (s) are tentative due to overlap of resonances.

the assignment of all resonances for the complex and the nucleotide base, H1′, H2′, and H2″ protons except the A_3-, A_7- and A_9-H2 resonances. Figure 2C shows the chemical shift changes observed for major and minor groove DNA protons. In this case, two distinct regions of change were observed to be T_2-A_3 and G_6-A_7.

Ten weak intermolecular NOEs were observed between the complex and the duplex, mostly between the picolyl protons of the complex and H1′ sugar protons of T_4, C_5, A_7, T_8, A_9, and T_{10} (Figure 4). No intermolecular NOE cross-peaks were observed involving the major groove AH8 or TCH_3 protons, even though these resonances displayed a number of intramolecular correlations.

Δ-cis-β-[Ru(RR-picchxnMe$_2$)(phen)]$^{2+}$−[d(CGCGATC-GCG)]$_2$ Adduct. To investigate the differences in DNA binding properties of the α- and β-isomers, a binding study of *β-phen* with [d(CGCGATCGCG)]$_2$ was undertaken. A ^{1}H NMR titration of the β-complex with the DNA (see Supporting Information) revealed that the aromatic DNA resonances are largely unaffected by the addition of the complex. Most notably, the minor groove A_5H2 proton signal, which shifts dramatically upfield in the presence of the α-isomer, remains unchanged in this case, indicating that binding does *not* occur in the central region from the minor groove.

2D NMR data were collected on the *β-phen*−[d(CGC-GATCGCG)]$_2$ adduct at a 2:1 ratio (0 °C), allowing complete assignment of all resonances for both the complex and the DNA. Upfield shifts were observed for all *phen* protons (Table 1), while the most significant changes for DNA resonances occur at the ends of the sequence (Figure 2D). A total of 27 intermolecular NOEs were observed between the β-complex and the ends of the oligonucleotide (Figure 5). NOE cross-peaks were observed to both major and minor groove proton resonances. Thus the complex:duplex binding stoichiometry for this adduct appears to be 2:1, with the complex binding to both ends of the duplex simultaneously.

Δ-cis-α-[Ru(RR-picchxnMe$_2$)(dpq)]$^{2+}$−[d(CGCGATC-GCG)]$_2$ Adduct. A ^{1}H NMR titration of the α-*dpq* complex with [d(CGCGATCGCG)]$_2$ at 40 °C (see Supporting Information) demonstrated an immediate upfield shift and broadening of the minor groove A_5H2 proton signal, together with downfield shifts of the A_5H8 and T_6H6 resonances. To assess the effects of increasing the bidentate surface area, the shielding of the bidendate protons was compared. Table 1 shows the upfield shifts of the *dpq* and picolyl proton

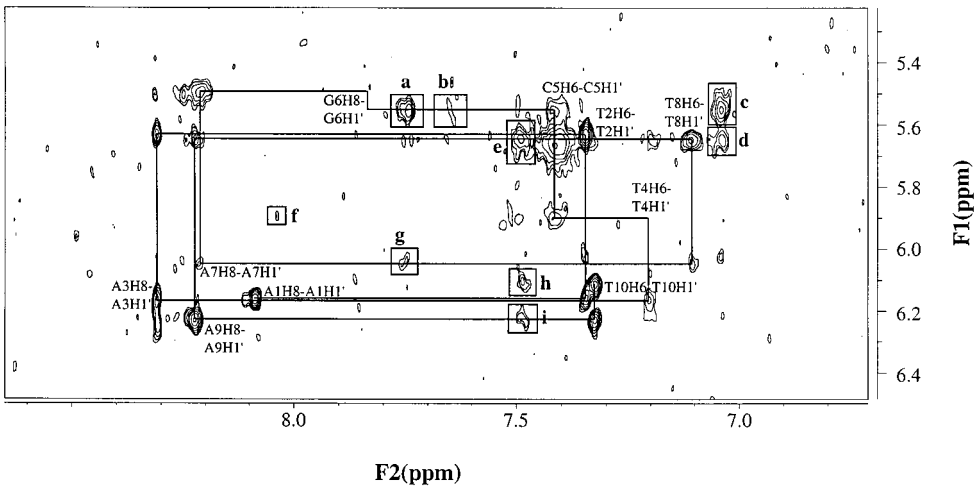

FIGURE 4: Portion of a ^{1}H NOESY spectrum (τ_m = 400 ms) of the α-*phen*−[d(ATATCGATAT)]$_2$ adduct at a 1:1 ratio (1.45 mM) at 40 °C. The solid line indicates the sequential H1′-H6/H8 correlations along the duplex. Due to multiple annealing the proton G_6H8 has partially exchanged with deuterium, resulting in a loss of intensity. The T_4H6-T_4H1′ cross-peak is also absent due to line broadening effects. The intermolecular NOEs between the complex and the duplex are shown in boxes. The labels correspond to NOEs between the following protons: (a) H5-C_5H1′, (b) H7-C_5H1′, (c) H6-C_5H1′, (d) H6-T_8H1′, (e) H8-T_8H1′, (f) H1-T_4H1′, (g) H5-A_7H1′, (h) H8-T_{10}H1′, and (i) H8-A_9H1′.

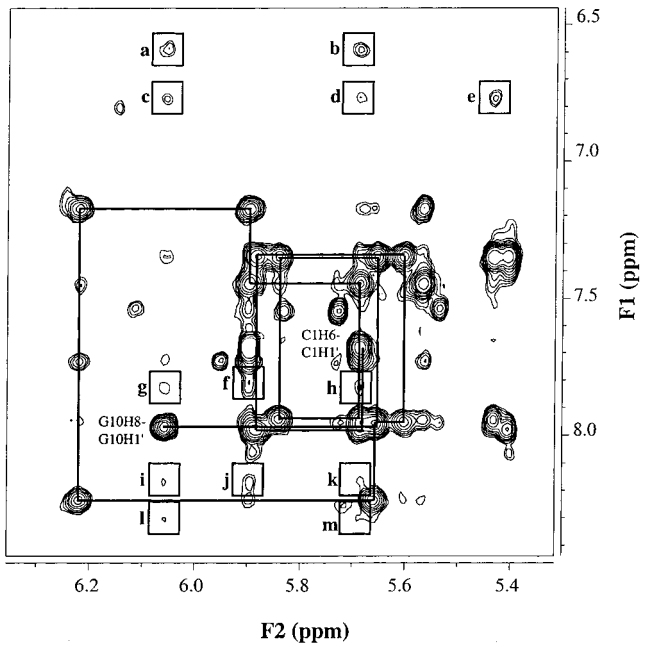

FIGURE 5: Portion of a ^{1}H NOESY spectrum ($\tau_m = 400$ ms) of the *β-phen*−[d(CGCGATCGCG)]$_2$ adduct at a 2:1 complex:duplex ratio ([DNA] = 1.25 mM) at 0 °C. The solid line indicates the H1′-H6/H8 sequential correlations observed along the duplex, while the intermolecular NOEs between the complex and the duplex are shown in boxes. The labels correspond to NOEs between the following protons: (a) H9-G_{10}H1′, (b) H9-C_1H1′, (c) H10-G_{10}H1′, (d) H10−C_1H1′, (e) H10-C_9H5, (f) H5-C_1H5/T_6H1′, (g) H1-G_{10}-H1′, (h) H1-C_1H1′, (i) H4-G_{10}H1′, (j) H4-C_1H5/T_6H1′, (k) H4-C_1-H1′, (l) H6-G_{10}H1′, and (m) H6-C_1H1′. Cross-peaks (f) and (j) are tentatively assigned because of severe overlap.

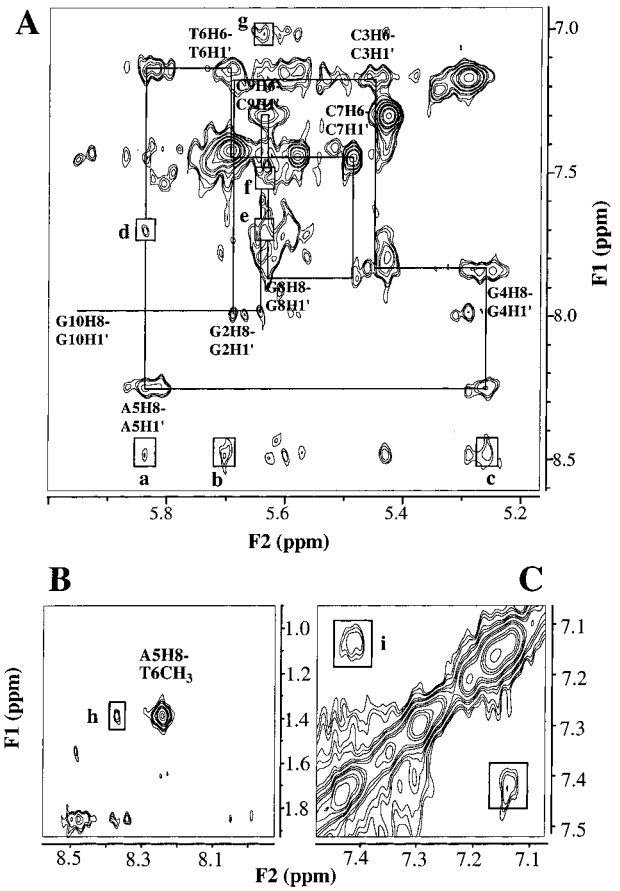

FIGURE 6: Portion of a ^{1}H NOESY spectrum of the α-*dpq*−[d(CGCGATCGCG)]$_2$ adduct at 40 °C (3.5:1 complex:duplex ratio, [DNA] = 0.57 mM, $\tau_m = 400$ ms) showing (A) the aromatic−H1′ region, (B) the aromatic−T(methyl) region, and (C) the aromatic−aromatic region. In (A), the solid line corresponds to the H1′-H6/H8 correlations along the duplex. The intermolecular NOEs between the complex and the duplex are shown in boxes. The labels correspond to NOEs between the following protons: (a) H3-A_5-H1′, (b) H3-T_6H1′, (c) H3-G_4H1′, (d) H5/H7-A_5H1′*, (e) H5/H7-C_9/G_8H1′, (f) H8-C_9/G_8H1′, (g) H6-C_9/G_8H1′, (h) H1-T_6CH_3, and (i) H2-T_6H6. Cross-peaks (e), (f), and (g) are only tentatively assigned.

resonances in the presence of DNA at 40 °C. As with the α-*phen* complex, the picolyl protons on the α-*dpq* complex only show minor chemical shift changes on binding to DNA.

Due to extreme broadening of the NMR resonances at room temperature for the DNA in the presence of α-*dpq*, 2D data were recorded at 60 °C. At this temperature, the DNA had not yet melted and signal resolution was reasonable. However, the GH8 and AH8 protons exchanged with the solvent (D_2O). Notably, A_5H8 exchanged only slowly at this temperature. The observed NOE cross-peaks also were very weak. Increasing the complex concentration (3.5:1) and lowering the temperature (40 °C) proved the best compromise. Under these conditions, nine clear intermolecular NOEs were observed (Figure 6 and Supporting Information), which were used to calculate a hypothetical molecular model. An energy-minimized (in vacuo) model of the adduct was calculated using a simple MM−MD−MM protocol, attributing a distance range of 1.8−5.0 Å for each observable NOE. Figure 7 shows the nine lowest energy structures (which contained no NOE violations) of the α-*dpq* complex intercalated at the G_4•C_7/A_5•T_6 site of a 5′-CGAT-3′ fragment from the minor groove. These calculations did not include the intermolecular NOEs observed to C_9, which most likely arise from the complex binding to the ends of the oligonucleotide, as was observed for α/*β-phen*. The existence of end stacking also is suggested by the substantial broadening of C_1•G_{10} proton resonances.

Δ-*cis*-α- *and* Δ-*cis*-*β*-*[Ru(RR-picchxnMe$_2$)(phi)]$^{2+}$ Adducts*. A titration of α-*phi* into a solution of [d(CGCGATCGCG)]$_2$ (see Supporting Information) resulted in an immediate broadening of the A_5H2, A_5H8, T_6H6, and C_7H6 resonances, with more widespread broadening as the titration progressed. The binding kinetics at 40 °C are on the slow exchange side of coalescence, but the adduct resonances were too broad to be observed. All aromatic resonances of the *phi* ligand undergo significant upfield shifts (Table 1). A smaller upfield shift (0.14 ppm) was observed for the imine protons.

2D NOESY data (0 °C) allowed the complete assignment of the DNA base, H1′, and H2′/2″ resonances of the adduct and assignment of approximately half of the complex resonances. Assignments for the complex resonances, however, were somewhat ambiguous due to their poor signal-to-noise ratios. Despite this, a number of intermolecular NOEs between the complex and the DNA could be discerned, involving major groove H2″ and CH5 resonances (data not shown). The pattern of intermolecular NOEs is concentrated around the G_4•C_7 base pair, and the sequential NOE correlations in the G_4•C_7/A_5•T_6 region are substantially reduced in intensity.

Similarly, when α-*phi* was titrated into a solution of [d(ATATCGATAT)]$_2$ (see Supporting Information) extensive

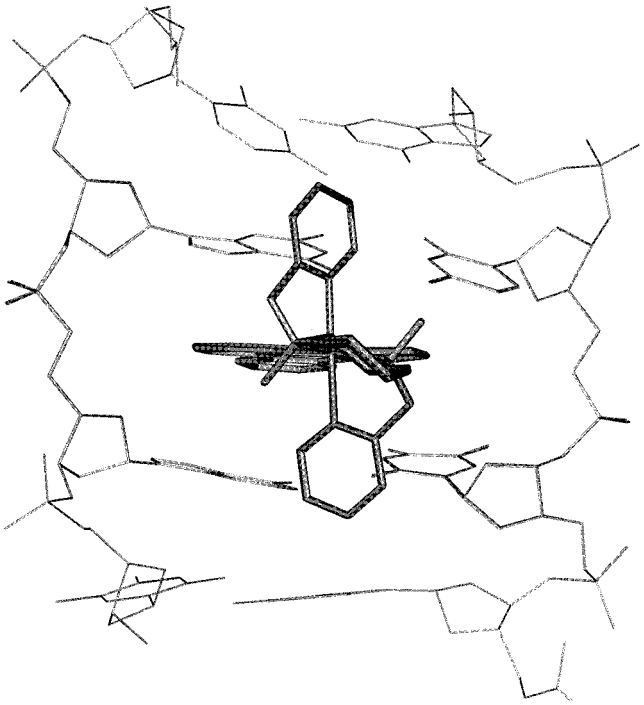

FIGURE 7: Energy-minimized model of α-*dpq* bound to the 5′-CGAT-3′ fragment of [d(CGCGATCGCG)]$_2$. The model shows the superposition of the nine lowest energy structures generated from 2 ns of MM−MD−MM (273 K), viewed from the minor groove.

broadening resulted throughout the ^{1}H NMR spectrum. In particular, all AT base protons (except A_1•T_{10}) underwent immediate broadening. Broadening of the complex resonances prevented the observation of intermolecular NOEs (τ_m = 400 ms, 30 °C). However, substantial reductions in the intensities of sequential NOEs (H2′/2″-base protons) involving the symmetrically equivalent T_2-A_3 and T_8-A_9 base steps (see Supporting Information) were observed.

The titration of *β-phi* into a sample of [d(CGCGATCGCG)]$_2$ (see Supporting Information) gave rise to immediate line broadening for the A_5H2, A_5H8, C_7H6, and T_6H6 resonances in a pattern virtually identical to that of the α-*phi* complex. Unfortunately, the line broadening displayed by this adduct precluded the observation of intermolecular NOEs.

Equilibrium Binding Affinities. Using the 1D NMR titration data, we were able to obtain estimates for the binding affinities of α-*phen* [$(1.0 \pm 0.1) \times 10^3$ M^{-1}], *β-phen* [$(1.4 \pm 0.1) \times 10^2$ M^{-2}], α-*dpq* [$(2.1 \pm 0.2) \times 10^3$ M^{-1}], and α-*phi* [$(4.7 \pm 1.3) \times 10^4$ M^{-1}] to [d(CGCGATCGCG)]$_2$. Binding constants for the three α-complexes were determined at 40 °C and for *β-phen* at 0 °C. Plots of the chemical shifts of selected DNA protons against the added volume of metal complex can be found in Supporting Information (A−C). The only signals chosen for the calculations were those clearly visible throughout the titration and which corresponded to protons close to the putative binding site of the complex in question. For α-*phen* and α-*dpq*, protons on the A_5 base were used (A_5H2 and A_5H8, respectively), while the end-stacking interaction of *β-phen* was monitored using G_{10}H1′. The α-*phi* binding affinity was obtained from a plot of the resonance of a proton on the metal complex (H4; Supporting Information D) against the added volume of oligonucleotide, owing to the extensive line broadening that occurs for the DNA resonances with added complex. The α-*phen*, α-*dpq*, and α-*phi* data were fitted to 1:1 binding models, reflecting the fact that, despite the likelihood of more than one possible binding site on the DNA, only one of these sites may be occupied at any one time. In addition, by carrying out these titrations at 40 °C, additional end-stacking interactions should be minimized. In contrast, the *β-phen* interaction was measured at 0 °C and fitted to a 2:1 binding model, under the assumption that the metal complexes could bind to both ends of the duplex simultaneously.

Thermal Denaturation Data. The relative magnitudes of the binding affinities measured above follow the same trend as the thermal denaturation data recorded for each of the complexes, in which the chemical shift of T_6CH_3 was monitored with increasing temperature (Figure 8A). Thus, the melting temperature of [d(CGCGATCGCG)]$_2$ bound to α-*phen*, *β-phen*, and α-*dpq* was observed to increase by 13, 7, and 21 °C, respectively, relative to free DNA. It is also notable that a second transition is observable in the melting curves for α-*phen* and α-*dpq* adducts below 40 °C. Data for the α-*phen* and α-*dpq* interactions are shown in Figure 8B, indicating that a second structural transition occurs at ∼10 and 27 ± 1 °C, respectively. In contrast, *β-phen* appears to show only a single transition. A complex:duplex ratio of 3.5:1 was used in order to ensure that most of the DNA was bound to the metal complex.

DISCUSSION

Metal Complexes. Complexation of the *picchxnMe$_2$* ligand with ruthenium can potentially give rise to a number of diastereoisomers, determined by the chirality of the tertiary cyclohexyl carbons (which can each be either *R* or *S*), the overall topology of the ligand (defined as either α or *β*), and the metal ion's absolute configuration (Δ or Λ) (*35*, *36*). In this study we have considered only the Δ-*RR* isomers of each complex. This absolute configuration was confirmed by ROESY (τ_m = 50 ms, 4 kHz spin lock) measurements for the α-*phen* cation where the calculated distances H10−H12a (2.64 Å) and H10−H12e (3.24 Å) agreed quantitatively with those of a model of the Δ-isomer (H10−H12a, 2.74 Å; H10−H12e, 3.35 Å) (*24*). For the alternative Λ-isomer, distances of 3.89 and 2.94 Å, respectively, would be expected. Further, the α-form has a C_2 symmetry, thereby halving the number of resonances observed in its NMR spectrum, in comparison with the asymmetric *β* form. The *N*-methyl groups on the *picchxnMe$_2$* ligand, which prevent oxidation to the monoimine form, also remove the potential for H-bonding of the cations to DNA (*36*). While DNA binding is controlled by strong ionic attractions, any site specificity should therefore be dominated by dispersive forces.

The appearance of NMR spectra during the DNA binding studies depends strongly on the kinetics of the particular interaction. In this study, all complexes were observed to be in either fast or intermediate exchange with the DNA, and chemical shift changes (Table 1) represent an average effect of the combined conformational changes and shielding/deshielding effects induced by the DNA when binding to the complex.

Thermal Denaturation. Thermal denaturation data can be used as evidence of small molecule binding to oligonucle-

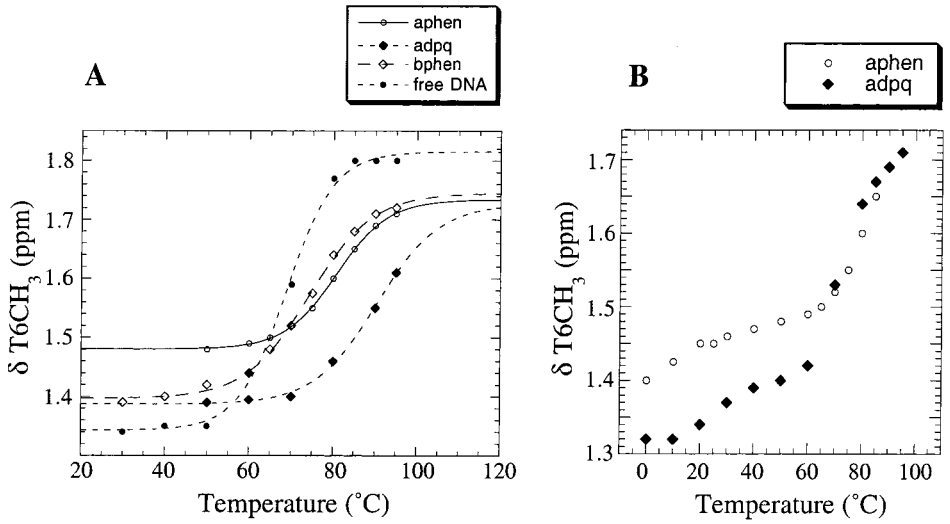

FIGURE 8: (A) Thermal denaturation data for $[d(CGCGATCGCG)]_2$ bound to α-*phen*, *β-phen*, and α-*dpq*. $\delta(T_6CH_3)$ is plotted against temperature at complex concentrations $R = 3.5$ for each adduct. The plot at $R = 0$ is included for comparison. The data have been fitted to a six-parameter sigmoidal curve fit. (B) Scatter plots of $\delta(T_6CH_3)$ in the presence of α-*phen* ($R = 3.5$) and α-*dpq* ($R = 1.0$).

otides and can be accurately measured by NMR spectroscopy (*37*). Increases in melting point (ΔT_m) of 5−16 °C have been observed by others for related complexes such as $[Rh(en)_2phi]^{3+}$ (*20*), Δ- and Λ-$[Ru(phen_2)dppz]^{2+}$ (*15*), and $Ru(phen)_3^{2+}$ (*2*). These values are also consistent with those observed for small molecule groove binders (*38*). The increase in ΔT_m observed from α-*phen* (+13 °C) to α-*dpq* (+21 °C) can be correlated to the relative surface area of the intercalating ligand. It is likely that the 7° increase in T_m observed for the *β-phen* complex is probably simply a consequence of the approximate doubling of the ionic strength of the solution that occurs when the ruthenium complex is added. It was not found possible to obtain an α-*phi*−$[d(CGCGATCGCG)]_2$ melting curve, due to the severe line broadening of T_6CH_3 upon addition of the cation, reflecting either a large ΔT_m or an alternative mode of binding. It should be noted that thermal denaturation data are generally not an indicator of binding affinity, as the temperature dependence of the K_b term is unknown.

Equilibrium Binding Affinities. The binding constant (K_b) is a direct measure of DNA affinity and increases from *phen* (1.0×10^3 M^{-1}) through *dpq* (2.1×10^3 M^{-1}) to *phi* (4.7×10^4 M^{-1}) for the α-complexes. Note, however, that the binding constants obtained for α-*phen* and α-*dpq* represent the affinities of the ruthenium complexes for a single site on the DNA (since they were measured by monitoring the chemical shift of a single DNA proton). These numbers may therefore be slightly underestimated, due to the existence of additional, weaker binding sites on the termini of the oligonucleotide. The K_b value observed for α-*phen* is comparable to binding constants reported for related metal complex−oligonucleotide interactions involving groove binding (*4*, *9*, *39*, *40*). The affinity measured for α-*dpq* is less than that expected for an intercalator. For example, Ru complexes with a *dppz* ligand exhibit DNA binding constants of 10^5−10^8 M^{-1} (*14*, *41*−*44*), although the *dppz* ligand has an additional aromatic ring that could increase its DNA binding affinity. Also, the *picchxnMe*$_2$ ligand may be involved in unfavorable steric interactions and, as noted earlier, must achieve secondary interactions only through dispersive forces.

The affinity measured for α-*phi* was higher than that for α-*phen* and α-*dpq* with the same oligonucleotide sequence but was still low for an intercalator where values of 10^5−10^{10} M^{-1} may be expected (*41*, *45*). The values are, however, qualitatively similar to those measured for these complexes using photometric hypochromism (*25*, *46*). Similar complexes (Ru and Rh complexes containing the *phi* ligand) have been reported with binding constants of 10^4−10^6 M^{-1} (*38*, *47*), while anthraquinone intercalators have been reported with binding constants of 10^4−10^5 M^{-1} (*48*). Our results are consistent with these but at the lower limit. This may be, in part, due to the nature of the *picchxnMe*$_2$ ligand as noted above but most likely is due to the way in which binding has previously been measured. For example, calf thymus DNA and other polynucleotides have a variety of potential binding sites with multiple binding possible. Through use of NMR spectroscopy and a short oligonucleotide, we are able to differentiate between central binding and end stacking for the α-*phen*, α-*dpq*, and *β-phen* adducts by observing only a single proton resonance on the oligonucleotide near the binding site. This NMR method has also recently been shown to give comparable results to more classical methods (*49*).

Metal Complex Chemical Shift Changes. The large upfield shift of H1 and H2 in the α-*phen* adduct suggests that the outermost protons are shielded by the DNA base stack. Such upfield shifts of *phen* protons upon DNA binding have been reported previously (*2*, *4*, *6*). In contrast, the shielding of the *β-phen* protons is variable and weak, inconsistent with intercalation. The *dpq* protons were affected in the order H2 > H1 > H3 > H4, indicating that H2 is in the region of greatest shielding by the DNA, consistent with data reported by Greguric et al. (*13*). This contrasts with the α-*phen* adduct, which shows the largest shielding for the H1 proton. It can be argued that these data provide evidence of intercalation because only when the pyrazine ring extends beyond the base pairs of the DNA can shielding of H1 be less than that of H2. An intercalative mode of binding for the *dpq* ligand has previously been suggested (*2*, *46*, *50*). For α-*phi*, the shielding of all aromatic phi protons upon mixing with DNA is consistent with intercalation (*47*, *51*, *52*). The relative degrees of shielding, H1 > H2 > H3 > H4, indicated that

H1 is not extended beyond the shielding zone of the DNA bases. For α-*phi*, the imine protons are only slightly shielded, suggesting that they lie outside the shielding zone of the base pairs. In all cases, the picolyl and aliphatic resonances on the *picchxnMe*$_2$ ligand are shifted only slightly, consistent with intercalation of the bidentate alone.

DNA Chemical Shift Changes and Intermolecular NOE Analysis. The complementary effect of the R complex upon DNA chemical shifts is more complicated. We have therefore used Figure 2 to graphically represent the effects of complex binding upon the DNA proton chemical shifts. For α-*phen* with [d(CGCGATCGCG)]$_2$ (Figure 2A), the greatest shielding occurs at the GA(T) region. Similarly, for α-*phen* with [d(ATATCGATAT)]$_2$ (Figure 2C), two sites of binding (TA and GA) are evident.

For α-*dpq* (Figure 2E), in comparison with the data for α-*phen* (Figure 2A), a qualitatively similar pattern emerges. Here, larger shifts for the minor groove central GA protons indicate a similar mode of binding. However, whereas the α-*phen* complex is in fast exchange with this oligonucleotide, the *dpq* complex exhibits intermediate exchange kinetics, resulting in substantial peak broadening throughout the spectrum. This would be indicative of a higher binding affinity (*4*). Similar exchange kinetics have been observed previously with the *dpq* ligand in metal complexes (*6*, *13*).

For α-*phen*, the strong NOEs between H6/H7 and C_7H1′ with [d(CGCGATCGCG)]$_2$ (Figure 4) are consistent with the *phen* ligand being positioned between the A_5•T_6 base pairs in the minor groove, whereas those between H4 and A_5H1′, C_7H1′, and G_4H1′ place the binding site between the G_4•A_5 base step. A number of other NOEs corroborate the conclusion that binding occurs at *both* of these central sites, albeit not simultaneously. Multiple binding modes have been noted previously with octahedral Ru complexes studied by ^{1}H NMR spectroscopy (*6*, *14*, *15*, *25*). It is notable that no major groove protons display NOEs to the Ru complex, despite displaying numerous intramolecular NOEs. An AT/GA preference is supported by the titrations of [ATATCGATAT]$_2$ with α-*phen* (Figure 2C). These results are consistent with minor groove binding between or adjacent to the several AT sites available in this duplex. Thus it is clear that the preferential AT/GA binding observed with the [d(CGCGATCGCG)]$_2$ sequence is not a result of higher stability of the central part of that oligonucleotide, a potential problem with shorter DNA duplex sequences.

There is no evidence for complete intercalation of α-*phen*, which would disrupt the sequential interbase cross-peaks at the binding site (*18*). A transition to A-DNA at the binding site can also be ruled out by the retention of the NOE pattern corresponding to a $C_{2'}$-*endo* pucker of the deoxyribose sugars (*34*). Instead, the combination of NOE data and chemical shift data (i.e., substantial shielding of *phen* and minor groove DNA resonances) is consistent with a model in which the bases separate in the minor but not the major groove, thus forming a wedge-shaped opening into which the outermost *phen* protons are inserted. In this model (*53*), the backbone conformation of the DNA is essentially unaltered. Similar binding modes have been previously described as "partial insertion" (*7*, *54*) and "semiintercalation" (*55*).

This minor groove binding is consistent with previous data reported for Δ-[Ru(phen)$_3$]$^{2+}$ bound to the same oligonucleotide sequence, which demonstrated a nonintercalative minor groove binding interaction (*3*, *4*, *6*). In contrast, a major groove intercalative interaction involving the same complex was reported by Rehmann and Barton (*2*), although this is not supported by our data.

For the *β-phen* isomer (Figure 2D), only stacking of the cation to the ends of the DNA is evident, as reflected in shielding of protons on the terminal residues. This is supported by NOE measurements (Figure 5), where the picolyl and *phen* protons display cross-peaks to both major and minor groove protons of the DNA, suggesting that the cation binds in several orientations. Specifically, NOEs from cation H9/H10 protons to terminal H1′ DNA protons place the axial picolyl ring in the minor groove, whereas NOEs from H9/H10 to DNA terminal H2′/2″ and C_9H5 protons place the axial picolyl ring in the major groove. In addition, NOEs from the complex methyl (H20) to DNA H1′ and H2″ protons place this group in both the DNA major and minor grooves, with the axial picolyl ring pointing *away* from the DNA. There are no intermolecular NOEs from the equatorial picolyl ring, indicating that it is pointing away from the DNA in all binding modes. The sequential H6/H8-H1′ NOE pattern is not disrupted at any step, indicating that there is no intercalation or DNA distortion occurring. Thus, there is a substantial difference in the DNA binding properties of α- and *β*-isomers of the *phen* complex. The *β*-isomer is presumably unable to fit into the minor groove, and it is interesting to note that this isomer does not appear to bind in the wider major groove as an alternative. These conclusions are supported by the low binding constant for *β-phen* and the marginal increase in T_m induced by binding.

A similar end-stacking interaction was observed for α-*phen* at 0 °C (Figure 2B, 3) where additional NOEs (c.f. at 40 °C) to the terminal C_1•G_{10} base pair are evident. A similar interaction has been noted previously with the binding of [Ru(phen)$_3$]$^{2+}$ to [d(CGCGATCGCG)]$_2$ at *R* values >1.0 (*4*) and for Λ- and Δ-*cis*-*β*-[Ru(*RR*-picchxn)(phen)]$^{2+}$ (*56*). The breakdown of this binding is reflected in Figure 8B for α-*phen* and α-*dpq*, which shows similar low-temperature events. NOESY spectra of the α-*phen*−[d(CGCGATCGCG)]$_2$ adduct recorded at higher temperatures do not contain cross-peaks from the terminal bases to the Ru complex, these only appearing at temperatures below 20 °C. Data to support such a second transition with other metal complexes have been published (*15*) but have not previously been interpreted as such. Likewise, the *β-phen* complex exhibits a very weak interaction with the ends of the DNA at 0 °C (K_b ∼140 M^{-1}). It is unlikely that the complex remains bound to the DNA once the temperature is raised above room temperature, and the most probable explanation for the increase in T_m that is observed in this case is that the ionic strength of the solution is increased substantially in the presence of the complex. This could result in stabilization of the DNA through nonspecific electrostatic interactions (in the same way that simple inorganic salts stabilize the double-stranded conformation for oligonucleotides).

In contrast to α-*phen*, α-*dpq* shows a genuine decrease in sequence-specific correlations between G_4 and A_5. However, it is difficult to establish whether there is a decrease in the H6/H8-H1′ sequence-specific NOEs in the central region of the oligonucleotide (Figure 6A), owing to the substantial spectral broadening observed (*6*, *15*). As there are two GA sites (one on each strand) in close proximity, it is unlikely

that both are bound simultaneously (*57*). The nonbound site would be expected to exhibit normal sequential NOE intensities.

Direct evidence for intercalation of α-*dpq* is provided by the aromatic−T(methyl) and aromatic−aromatic regions of the NOESY spectrum (Figure 6). Cation protons H1 and H2 show intermolecular NOEs to the major groove protons T_6-CH_3 and T_6H6, respectively (Figure 6B,C), whereas the picolyl and *dpq* H3 protons display NOEs to minor groove H1′ protons. These data are consistent with intercalation from the minor groove at the G_4A_5 step, with the outermost *dpq* H1 and H2 protons extended through the duplex into the major groove.

Both α-*phi* and *β*-*phi* display similar effects on the oligonucleotide, with immediate broadening of major groove base protons in the A_5, T_6, and C_7 region, disruption of the sequence-specific H6/8-H1′ NOEs in the G_4-C_7 region, and intermolecular NOEs from Ru complex protons to C_7H5 and several H2″ protons. Taken together, these data are consistent with intercalation from the major groove in the central AT region of the oligonucleotide. However, because of the broadness of the NMR spectra, we were unable to determine the precise site of intercalation. Indeed, more than one site may exist. A preference for AT was confirmed by titrating α-*phi* with $[d(ATATCGATAT)]_2$ where broadening was observed for the $T_2{\cdot}A_9/A_3{\cdot}T_8$ major groove protons. This similarity between α- and *β*-isomers contrasts with our observations on the *phen* complexes, where the shape of the *β*-isomer inhibits binding in the center of the DNA sequence.

Δ-cis-α-[Ru(RR-picchxnMe$_2$)(dpq)]$^{2+}$−DNA Molecular Model. Because of severe line broadening due to intermediate exchange kinetics, it was not possible to assign all of the DNA signals with certainty. Also, the broadening made integration of intra- and intermolecular NOEs difficult. Under these circumstances, modeling began with a high-resolution crystal structure of actinomycin bound to an oligonucleotide. Replacement of the actinomycin by α-*dpq* was the starting point for modeling. As the ESFF force field treated DNA poorly (but was parametrized for Ru), it was necessary to keep the DNA fixed during initial MM and MD, only releasing the DNA atoms for the final MM. On the basis of the nine intermolecular NOEs observed, a molecular model was constructed that is consistent with these and results published for Δ-$[Ru(phen)_2dpq]^{2+}$ bound to $[d(GTCGAC)]_2$ and $[d(TCGGGATCCCGA)]_2$ (*6*, *13*). Both complexes display intercalation from the minor groove at purine−purine/pyrimidine−pyrimidine sites, and both show NOEs from the outermost *dpq* protons to major groove DNA protons on a thymine base. While the data in Figure 7 are consistent with the NOEs observed, this tentative model was not well enough restrained by the experimental data to allow detailed conclusions to be drawn on changes to the DNA structure. However, repeating the calculations for intercalation from the major groove or from any other base pair other than the $G_4{\cdot}C_7/A_5{\cdot}T_6$ site results in multiple restraint violations. The structure also accounts for the relative deshielding of cation H1 (Table 1) and the shielding of minor groove G_4 and A_5 protons (Figure 2E).

Complementarity of the phi Ligand with the DNA Major Groove. To account for the apparent groove specificity and loss of configurational discrimination for the *phi* complexes, we examined molecular models of intercalation sites from crystallographic data. The shape of a DNA intercalation site, though flexible, is distinctly trapezoidal, with its widest edge on the major groove side (Figure 9). This shape, combined with the widths of the DNA major (11.7 Å) and minor (5.7 Å) grooves (*58*) and the width (10.5 Å) and shape of the *phi* ligand, supports the conclusion that DNA binding for the *phi* complexes must occur from the major groove. In this orientation, the van der Waals fit between DNA and *phi* is substantially better and avoids the steric overlap between H3 of the *phi* ligand and either O4′ (the ribose ring oxygen) or H2′ on the other side of the intercalation site.

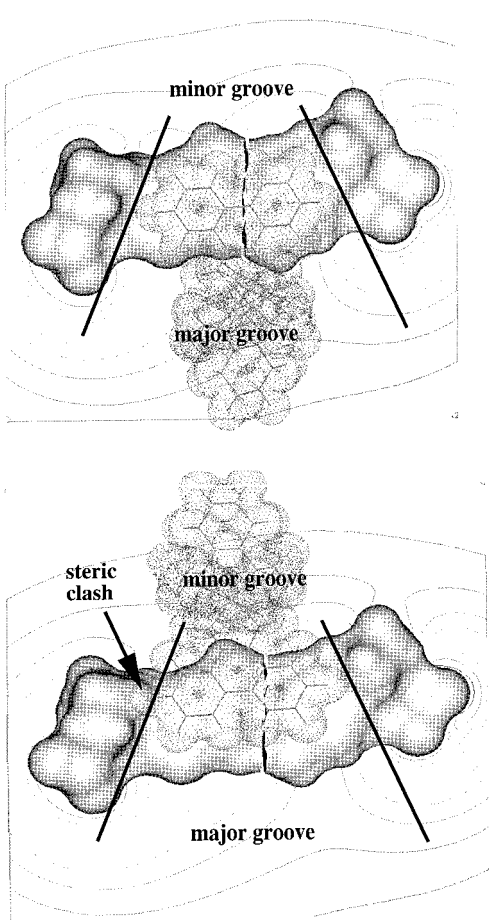

FIGURE 9: A base pair fragment with α-*phi* intercalated from (A) the major groove and (B) the minor groove. The intercalation site, viewed down the symmetry axis of the DNA, is rendered with a Connolly surface (sphere radius 1.4 Å) and the complex with a van der Waals surface. An isoelectric potential slice through the intercalation site is diplayed as contours. Note the complementary fit of the *phi* ligand when binding occurs from the major groove and the steric mismatch when binding occurs from the minor groove.

Overview of the Metal Complex−DNA Interactions. At the conclusion of this study, various DNA binding characteristics of the complexes are evident. First, differences in the DNA binding modes of the complexes were observed. The α-*phen* complex exhibits predominantly a groove binding interaction but shows some characteristics of intercalation. Our results suggest that the *phen* ligand is "partially inserted" (*53*) between the base pairs without causing substantial base pair separation. Complexes containing the *dpq* and *phi* ligands show evidence of true intercalation between the DNA base pairs, both from the intermolecular NOE pattern and from DNA stabilization. Second, distinct

DNA groove discrimination was observed in the binding characteristics of different complexes. The α-*phen* and α-*dpq* complexes both show unequivocal binding from the minor groove, which is not surprising given the similarity of their structure and the simple addition of a pyrazine ring to the intercalating bidentate (i.e., going from *phen* to *dpq*). Continuing this argument, by addition of another benzene ring, groove selectivity should not be changed, and we predict that α-*dppz* should also intercalate from the minor groove. In contrast, the *phi* complexes showed evidence of major groove binding. The *β*-*phen* complex shows only evidence of a weak, end-stacking interaction, indicating that the *β*-*picchxnMe*$_2$ ligand does not fit into the minor groove. Third, the complexes exhibit marked DNA sequence selectivity for the oligonucleotide strands studied. The α-*phen* complex shows a preference for AT, TA, and GA sites, as well as end stacking at low temperature. The α-*dpq* complex displays a preference for intercalation at a GA site, indicating that extension of the bidentate moiety produces a more specific interaction. The α- and *β*-*phi* complexes each show evidence of TA/AT sequence selectivity.

An overwhelming observation in this study is the preference for GA and TA/AT DNA binding sites and the marked lack of affinity for CG or GC sites. In the minor groove, the electrostatic potentials are considerably more negative for AT sequences than for GC sequences (*59*), and thus it is likely that a small cationic DNA binding molecule will be attracted initially to the AT minor groove. This is indeed our result for the α-*phen* and α-*dpq* complexes. This point has been noted previously in the binding of Δ-[Ru(phen)$_3$]$^{2+}$ to the AT minor groove of [d(CGCGATCGCG)]$_2$ (*4*) and in molecular modeling studies of trypanocide guanyl hydrazones bound to minor groove AT-rich regions (*60*). The presence of a G base on the 5′ side of the AT site offers a more significant opportunity for drug design as it provides scope for chemical tuning of the binding, rather than simply electrostatic attraction to the region of most negative potential, as is the case with other AT-specific minor groove binders.

The *β*-stereochemistry of these metal complexes does not appear to be compatible with binding in either the DNA major or DNA minor grooves when combined with the *phen* ligand. The only binding position that can be accommodated is an aromatic stacking interaction with the ends of the DNA. It appears that *β*-*picchxnMe*$_2$ is incompatible with minor groove binding for steric reasons, as inspection of a model suggests that both methyl groups on the *β*-*picchxnMe*$_2$ ligand may clash with the DNA backbone and that the overall shape of the tetradentate ligand is not complementary to the DNA minor groove. It is interesting to speculate why the *β*-*phen* complex does not bind in the major groove (as the *β*-*phi* complex does), and it is most probably due to the lack of aromatic overlap between the *phen* ligand and the DNA base pairs, as the *phen* ligand does not extend out from the metal center as far as the *phi* ligand.

α-*phi* has been shown to bind to [d(CGCGATCGCG)]$_2$ by intercalation from the major groove. Furthermore, *β*-*phi* also binds to [d(CGCGATCGCG)]$_2$, showing changes in the 1D NMR spectra nearly identical to the α-*phi*−[d(CGCGATCGCG)]$_2$ adduct. These results are consistent with previous work on these Ru complexes with calf thymus DNA (*25*). This loss of discrimination between α- and *β*-isomers could be occurring for two reasons. First, the major groove may be wide enough to accommodate the *picchxnMe*$_2$ ligand in both the α- and *β*-conformations. It appears that, to operate effectively as a sequence-selective binding agent, the *picchxnMe*$_2$ ligand must be able to form van der Waals contacts with the DNA groove, and this is most likely to occur if DNA binding occurs from the significantly narrower minor groove. Second, the tetradentate ligand may be further from the DNA groove because of the larger *phi* ligand. Both of these factors result in the removal of the shape-selective discrimination provided by the *picchxnMe*$_2$ ligand and leave open the possibility that the presence of the *picchxnMe*$_2$ ligand in both the α- and *β*-*phi* complexes is largely redundant. Note that the *phi* complexes *do* appear to exhibit overall sequence selectivity for major groove TA/AT sites but that this is most likely not due to the *picchxnMe*$_2$ ligand. It is proposed that the complementary shape of the *phi* ligand with a major groove intercalation site is responsible for the groove selectivity, and this alone explains why *phi* is universally reported as a major groove binder whereas other ligands of substantially different geometry, such as *phen* and *dpq*, show evidence of minor groove binding. An earlier paper by Barton (*51*) reported CG selectivity for Δ-[Rh(phen)$_2$phi]$^{3+}$ and [d(GTCGAC)]$_2$ and relied heavily on an NOE between T_2CH_3 and the H1 of the *phi* ligand. However, the chemical shift of this methyl (δ 1.5) suggests that the DNA is single stranded [c.f. δ 1.34 for double-stranded DNA in [d(GTCGAC)]$_2$]. This is supported by our own measurements of T_m for this hexamer (45 °C). The NMR data reported by Barton were recorded at 47 °C, and even allowing for an increase in T_m afforded by binding of the complex, due to thermal fraying of the oligonucleotide, it is inconceivable that anything but the central GC region was actually duplex. Consequently, no other binding opportunity exists under these conditions, and it remains a distinct possibility that the complex under study would have shown a preference for whatever sequence was at the center of the duplex. We suggest that the trapezoidal shape of the intercalating ligand can shift the preference from major to minor grooves in otherwise similar molecules. The *phen* and *phi* ligands are similar except reversed in their attachment to the metal. This reversal also reverses the groove binding selectivity of the complex, independent, in this case, of the ancillary ligands.

ACKNOWLEDGMENT

We gratefully acknowledge the Universities of Sydney and NSW for access to their respective 600 MHz NMR facilities. We thank Dr. G. Ball (University of New South Wales) and Mr. K. Tonkin (Macquarie University) for assistance with NMR measurements and Dr. W. Kett (Macquarie University) for assistance with HPLC. The α-/*β*-*phen* and α-/*β*-*phi* complexes used in this study were synthesized by Dr. K. Vickery (Macquarie University), and the α-*dpq* complex was synthesized by Mrs. L. Sutherland (Macquarie University) from *dpq* ligand supplied by Dr. I. Greguric and Dr. J. Aldrich-Wright (University of Western Sydney). We also thank Prof. Robert Vagg for critically reviewing the manuscript and Profs. Robert Vagg and Peter Williams, whose research and ideas laid the groundwork for these results.

SUPPORTING INFORMATION AVAILABLE

A total of 11 supplementary figures, including free and bound DNA assignments, 1D NMR titrations, intermolecular NOE list for the α-*phen*−[d(CGCGATCGCG)]$_2$ adduct, α-*dpq*−[d(CGCGATCGCG)]$_2$ model coordinate file in PDB format, calculated distances for the α-*dpq*−[d(CGCGATCGCG)]$_2$ model, NOESY spectrum of the α-*phi*−[d(ATATCGATAT)]$_2$ adduct, and plots of chemical shift vs *R*-value for the binding affinity calculations. This material is available free of charge via the Internet at http://pubs.acs.org.

REFERENCES

1. Erkkila, K. E., Odom, D. T., and Barton, J. K. (1999) *Chem. Rev. 99*, 2777−2795.
2. Rehmann, J. P., and Barton, J. K. (1990) *Biochemistry 29*, 1701−1709.
3. Eriksson, M., Leijon, M., Hiort, C., Norden, B., and Graslund, A. (1992) *J. Am. Chem. Soc. 114*, 4933−4934.
4. Eriksson, M., Leijon, M., Hiort, C., Norden, B., and Graslund, A. (1994) *Biochemistry 33*, 5031−5040.
5. Norden, B., Patel, N., Hiort, C., Graslund, A., and Kim, S. K. (1991) *Nucleosides Nucleotides 10*, 195−205.
6. Collins, J. G., Sleeman, A. D., Aldrich-Wright, J. R., Greguric, I., and Hambley, T. W. (1998) *Inorg. Chem. 37*, 3133−3141.
7. Haworth, I. S., Elcock, A. H., Freeman, J., Rodger, A., and Richards, W. G. (1991) *J. Biomol. Struct. Dyn. 9*, 23−44.
8. Barton, J. K., Goldberg, J. M., Kumar, C. V., and Turro, N. J. (1986) *J. Am. Chem. Soc. 108*, 2081−2088.
9. Satyanarayana, S., Dabrowiak, J. C., and Chaires, J. B. (1993) *Biochemistry 32*, 2573−2584.
10. Hiort, C., Norden, B., and Rodger, A. (1990) *J. Am. Chem. Soc. 112*, 1971−1982.
11. Yamagishi, A. (1983) *J. Chem. Soc., Chem. Commun.*, 572−575.
12. Akasheh, T. S., Marji, D., and Al-Ahmed, Z. M. (1988) *Inorg. Chim. Acta 141*, 125−130.
13. Greguric, I., Aldrich-Wright, J. R., and Collins, J. G. (1997) *J. Am. Chem. Soc. 119*, 3621−3622.
14. Dupureur, C. M., and Barton, J. K. (1994) *J. Am. Chem. Soc. 116*, 10286−10287.
15. Dupureur, C. M., and Barton, J. K. (1997) *Inorg. Chem. 36*, 33−43.
16. Holmlin, R. E., Stemp, E. D. A., and Barton, J. K. (1998) *Inorg. Chem. 37*, 29−34.
17. Tuite, E., Lincoln, P., and Norden, B. (1997) *J. Am. Chem. Soc. 119*, 239−240.
18. Hudson, B. P., and Barton, J. K. (1998) *J. Am. Chem. Soc. 120*, 6877−6888.
19. Kielkopf, C. L., Erkkila, K. E., Hudson, B. P., Barton, J. K., and Rees, D. C. (2000) *Nat. Struct. Biol. 7*, 117−121.
20. Shields, T. P., and Barton, J. K. (1995) *Biochemistry 34*, 15049−15056.
21. Franklin, S. J., and Barton, J. K. (1998) *Biochemistry 37*, 16093−16105.
22. Krotz, A. H., Kuo, L. Y., Shields, T. P., and Barton, J. K. (1993) *J. Am. Chem. Soc. 115*, 3877−3882.
23. Shields, T. P., and Barton, J. K. (1995) *Biochemistry 34*, 15037−15048.
24. Proudfoot, E. M., Mackay, J. P., Vagg, R. S., Vickery, K. A., Williams, P. A., and Karuso, P. (1997) *Chem. Commun. (Cambridge)*, 1623−1624.
25. Murphy-Poulton, S. F., Vagg, R. S., Vickery, K. A., and Williams, P. A. (1998) *Met.-Based Drugs 5*, 225−231.
26. Fenton, R. R., Stephens, F. S., Vagg, R. S., and Williams, P. A. (1991) *Inorg. Chim. Acta 182*, 67−75.
27. Vickery, K. A. (1998) Ph.D. Thesis, Macquarie University.
28. Sambrook, J., Fritsch, E. F., and Maniatis, T. (1989) *Molecular Cloning: A Laboratory Manual*, Cold Spring Harbor Laboratory Press, Cold Spring Harbor, NY.
29. Wuthrich, K. (1986) *NMR of Proteins and Nucleic Acids*, Wiley, New York.
30. Connors, K. A. (1987) *Binding Constants: The Measurement of Molecular Complex Stability*, John Wiley and Sons, New York.
31. Kamitori, S., and Takusagawa, F. (1992) *J. Mol. Biol. 225*, 445.
32. Barlow, S., Rohl, A. L., Shi, S., Freeman, C. M., and O'Hare, D. (1996) *J. Am. Chem. Soc. 118*, 7578−7592.
33. Barlow, S., Rohl, A. L., and O'Hare, D. (1996) *Chem. Commun.*, 257−260.
34. Watt, T. A., Tong, C., Arnold, A. P., and Collins, J. G. (1996) *Biochem. Mol. Biol. Int. 38*, 383−391.
35. Shimura, Y. (1982) *Kagaku 37*, 80−82.
36. Aldrich-Wright, J. R., Vagg, R. S., and Williams, P. A. (1997) *Coord. Chem. Rev. 166*, 361−389.
37. Berman, H. M., and Young, P. R. (1981) *Annu. Rev. Biophys. Bioeng. 10*, 87−114.
38. Pyle, A. M., Rehmann, J. P., Meshoyrer, R., Kumar, C. V., Turro, N. J., and Barton, J. K. (1989) *J. Am. Chem. Soc. 111*, 3051−3058.
39. Watt, T. A., Collins, J. G., and Arnold, A. P. (1994) *Inorg. Chem. 33*, 609−610.
40. Satyanarayana, S., Dabrowiak, J. C., and Chaires, J. B. (1992) *Biochemistry 31*, 9319−9324.
41. Hiort, C., Lincoln, P., and Norden, B. (1993) *J. Am. Chem. Soc. 115*, 3448−3454.
42. Haq, I., Lincoln, P., Suh, D., Norden, B., Chowdhry, B. Z., and Chaires, J. B. (1995) *J. Am. Chem. Soc. 117*, 4788−4796.
43. Gupta, N., Grover, G. A., Neyhart, G. A., Liang, W., Singh, P., and Thorp, H. H. (1992) *Angew. Chem., Int. Ed. Engl. 31*, 1048−1050.
44. Nair, R. B., Teng, E. S., Kirkland, S. L., and Murphy, C. J. (1998) *Inorg. Chem. 37*, 139−141.
45. Pindur, U., Haber, M., and Sattler, K. (1993) *J. Chem. Educ. 70*, 263−272.
46. Vickery, K. A., Bonin, A. M., Vagg, R. S., and Williams, P. A. (1997) in *Struct., Motion, Interact. Expression Biol. Macromol., Proc. Conversation Discip. Biomol. Stereodyn., 10th* (Sarma, R. H., and Sarma, M. H., Eds.) pp 195−205, Adenine Press, Schenectady, NY.
47. Naing, K., Takahashi, M., Taniguchi, M., and Yamagishi, A. (1995) *Inorg. Chem. 34*, 350−356.
48. Haq, I., Ladbury, J. E., Chowdhry, B. Z., and Jenkins, T. C. (1996) *J. Am. Chem. Soc. 118*, 10693−10701.
49. Collins, J. G., Aldrich-Wright, J. R., Greguric, I. D., and Pellegrini, P. A. (1999) *Inorg. Chem. 38*, 5502−5509.
50. Long, G. V., Harding, M. M., Fan, J.-Y., and Denny, W. A. (1997) *Anti-Cancer Drug Des. 12*, 453−472.
51. David, S. S., and Barton, J. K. (1993) *J. Am. Chem. Soc. 115*, 2984−2985.
52. Collins, J. G., Shields, T. P., and Barton, J. K. (1994) *J. Am. Chem. Soc. 116*, 9840−9846.
53. Coggan, D. Z. M., Haworth, I. S., Bates, P. J., Robinson, A., and Rodger, A. (1999) *Inorg. Chem. 38*, 4486−4497.
54. Haworth, I. S., Elcock, A. H., Rodger, A., and Richards, W. G. (1991) *J. Biomol. Struct. Dyn. 9*, 553−569.
55. Lincoln, P., and Norden, B. (1998) *J. Phys. Chem. B 102*, 9583−9594.
56. Vickery, K., Vagg, R., Lincoln, P., Norden, B., and Eriksson, M. (1999) *J. Biomol. Struct. Dyn. 17*, 519−525.
57. Franklin, S. J., Treadway, C. R., and Barton, J. K. (1998) *Inorg. Chem. 37*, 5198−5210.
58. Saenger, W. (1984) *Principles of Nucleic Acid Structure*, Springer-Verlag, New York.
59. Lavery, R., and Pullman, B. (1981) *Int. J. Quantum Chem. 20*, 259−272.
60. Santos-Filho, O. A., and Figueroa-Villar, J. D. (1997) *Bioorg. Med. Chem. Lett. 7*, 1797−1802.

BI001655F